Electronic Supplementary Information (ESI)

Pentagonal two-dimensional noble-metal dichalcogenides PdSSe for photocatalytic water splitting with pronounced optical absorption and ultrahigh anisotropic carrier mobility

Feng Xiao,[1] Wen Lei,[1,2] Wei Wang,[1] Lili Xu,[3] Shengli Zhang,[3*] and Xing Ming[1,4*]

1. College of Science, Guilin University of Technology, Guilin 541004, PR China

2. Key Laboratory of Artificial Micro- and Nano-Structures of Ministry of Education and School of Physics and Technology, Wuhan University, Wuhan 430072, PR China

3. MIIT Key Laboratory of Advanced Display Materials and Devices, School of Materials Science and Engineering, Nanjing University of Science and Technology, Nanjing 210094, PR China.

4.MOE Key Laboratory of New Processing Technology for Nonferrous Metal & Materials, Guilin University of Technology, Guilin 541004, China

Email: mingxing@glut.edu.cn (Xing Ming) zhangslvip@njust.edu.cn (Shengli Zhang)

1. The choice of the semiempirical correction methods

Considering that PdSSe, as isomorphous intermediate of $PdSe_2$ and PdS_2, adopts layered five-membered ring structure and van der Waals interaction exists along the *c* axis layer-stacking direction. In order to apply appropriate correction methods to PdSSe crystals, we employ the correction method, Tkatchenko-Scheffler method (PBE-TS), which is applicable to both the PdS_2 and $PdSe_2$. In **Table S1** and **Table S2**, our theoretical calculated lattice parameters with different methods of correction are compared with previous experimental data and calculation results. As for the optimized $PdSe_2$ lattices, the error of IHP-PBE-TS, PBE-MBD and PBE-TS methods is very small, but the first two methods slightly overestimate the lattice constant *c* of PdS_2. Compared with the other correction methods, PBE-TS method performs well in optimizing PdS_2 and $PdSe_2$ with small errors. Used to optimize PdSSe, the theoretical results are consistent with the experimental results, shown in **Table 1** in the main text, implying the validity of our choice with the PBE-TS method.

Table S1 Calculated lattice constants and cell volume for the PdS_2 compared with experimental data.

PdS_2	Lattice constant			Volume	Relative error (%)			
	a(Å)	b(Å)	c(Å)	V(Å^3)	△a/a	△b/b	△c/c	△V/V
Expt.[1]	5.460	5.541	7.531	227.842	-	-	-	-
PBE	5.487	5.579	8.718	266.880	0. 5	0. 7	15.8	17.1
PBE-sol	5.442	5.524	7.546	226.859	0. 3	0. 3	0. 2	0. 4
LDA	5.454	5.515	7.016	211.045	0. 1	0. 5	6.8	7.4
DFT-D3(Grimme)	5.513	5.577	7.100	218.328	1.0	0. 7	5.7	4.2
PBE-dDsC	5.478	5.562	7.592	231.304	0. 3	0. 4	0. 8	1.5
PBE-D2	5.481	5.558	7.616	232.047	0. 4	0. 3	1.1	1.8
PBE-D3(BJ)	5.508	5.576	7.474	229.497	0. 9	0. 6	0. 8	0. 7
IHP_PBE-TS	5.499	5.578	8.035	246.455	0. 7	0. 7	6.7	8.2
PBE-MBD	5.484	5.574	7.771	237.551	0. 4	0. 6	3.2	4.3
PBE-TS	5.515	5.588	7.691	237.038	1.0	0. 8	2.1	4.0
optB86b	5.672	5.757	8.121	265.198	3.9	3.9	7.8	16.4
optP88	5.496	5.580	7.458	228.715	0. 7	0. 7	1.0	0. 4
optPBE	5.523	5.608	7.619	236.012	1.2	1.2	1.2	3.6

Table S2 Calculated lattice constants and cell volume for the $PdSe_2$ compared with experimental data.

$PdSe_2$	Lattice constant			Volume	Relative error (%)			
	a(Å)	b(Å)	c(Å)	V(Å^3)	△a/a	△b/b	△c/c	△V/V
Expt.[1]	5.741	5.866	7.691	259.01	-	-	-	-
PBE	5.782	5.933	8.588	294.658	0. 7	1.2	11.7	13.8
PBE-sol	6.178	6.135	6.148	233.044	7.6	4.6	20.1	10
LDA	6.094	6.099	6.099	226.669	6.1	4	20.7	12.5
DFT-D3(Grimme)	6.218	6.166	6.167	236.452	8.3	0.051	19.8	8.7
PBE-dDsC	5.851	5.949	7.337	255.403	1.9	1.4	4.6	1.4
PBE-D2	6.194	6.204	6.191	237.897	7.9	5.8	19.5	8.2
PBE-D3(BJ)	5.897	5.956	7.16	251.517	2.7	1.5	6.9	2.9
IHP_PBE-TS	5.853	5.95	7.728	269.139	2	1.4	0. 5	3.9
PBE-MBD	5.821	5.939	7.644	264.28	1.4	1.2	0.6	2
PBE-TS	5.857	5.95	7.713	268.78	2	1.4	0. 3	3.8
optB86b	6.006	6.144	8.389	309.516	4.6	4.7	9.1	19.5
optP88	6.323	6.197	6.157	241.259	10.1	5.6	19.9	6.9
optPBE	5.891	5.999	7.486	264.518	2.6	2.3	2.7	2.1

2. The phonon spectrum and electronic structure of bulk PdSSe

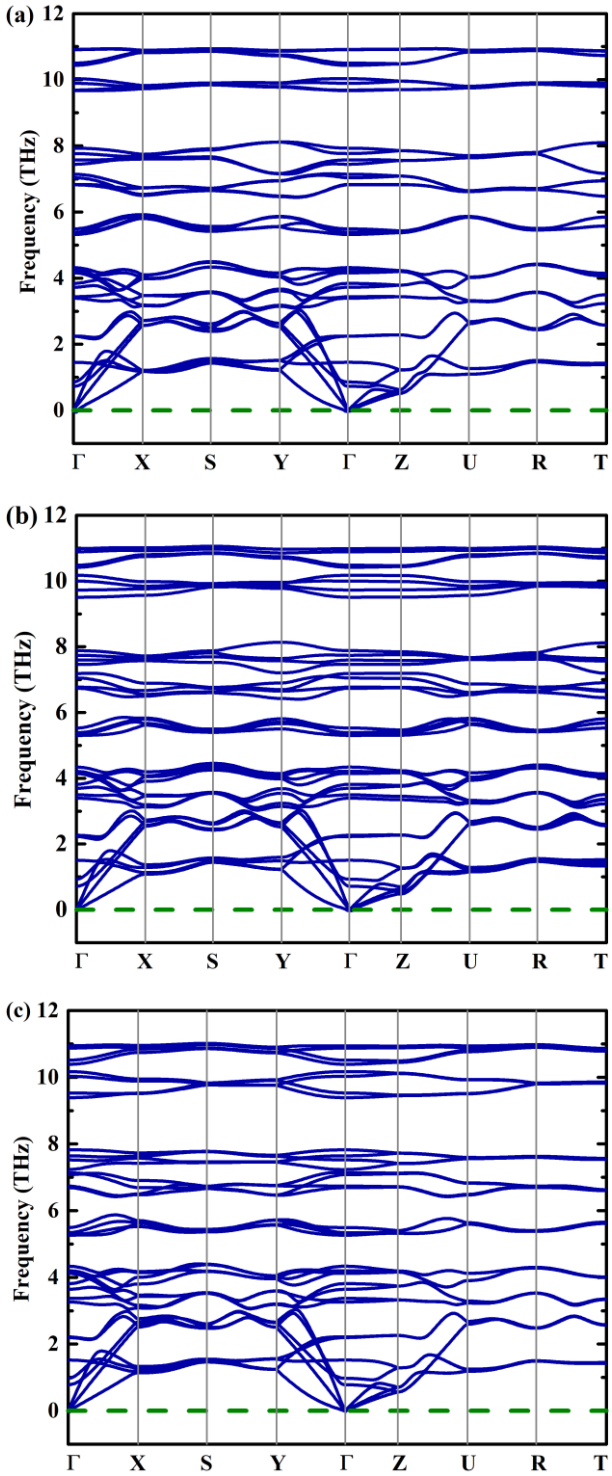

Figure S1 The phonon spectra along the high-symmetry lines for bulk phases of (a) *AA*, (b) *AB* and (c) *BB* polymorphs.

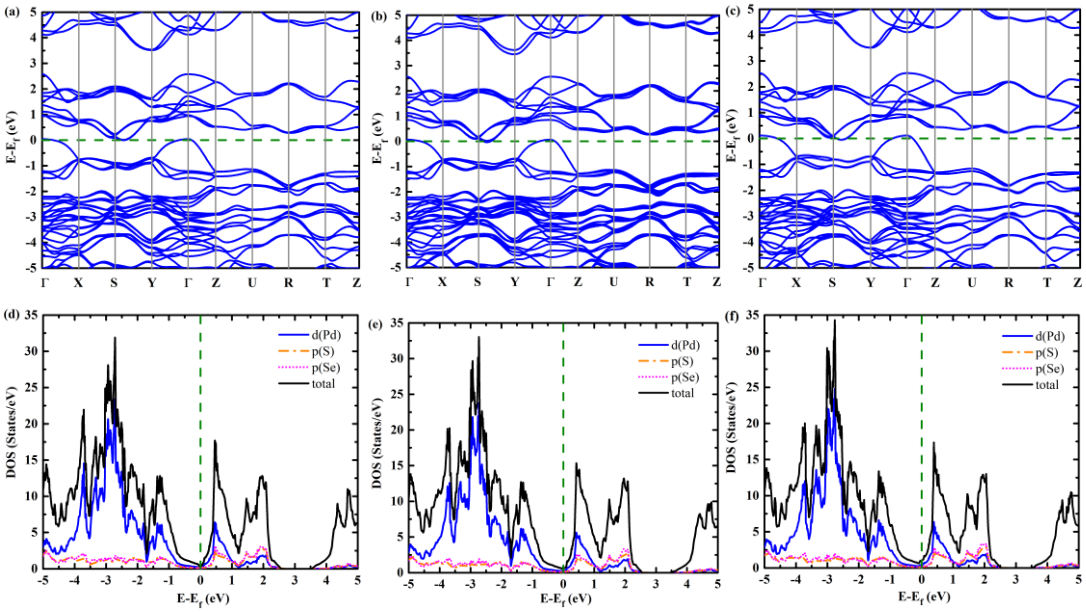

Figure S2 Band structure of the bulk phases PdSSe of (a) *AA*, (b) *AB*, (d) *BB* polymorphs, and the corresponding density of states for (d) *AA*, (e) *AB*, (f) *BB* polymorphs calculated with PBE.

3. Exfoliation of 2D monolayer PdSSe from bulk

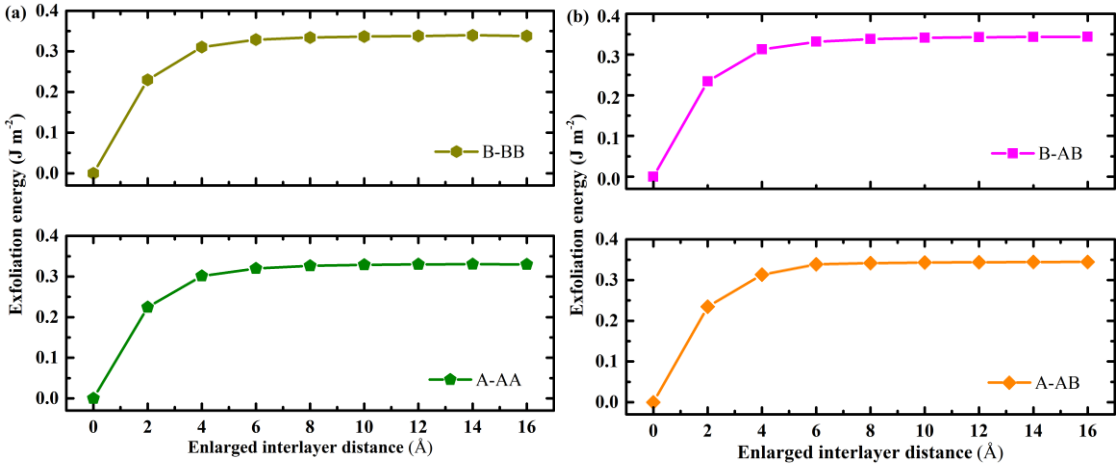

Figure S3 The exfoliation energy estimation for monolayer PdSSe from (a) *AA* or *BB* bulk and (b) *AB* bulk.

Table S3 The energy required to exfoliate PdSSe monolayer from their corresponding bulk phases, which are compared with the exfoliation energy of isostructural monolayer PdS_2 and $PdSe_2$.

Type of monolayer	provenance	$E_{exfl.}$(J m^{-2})
A	*AA*	0.330
	AB	0.345
B	*AB*	0.343
	BB	0.338
PdS_2[2]		0.31
$PdSe_2$[2]		0.33

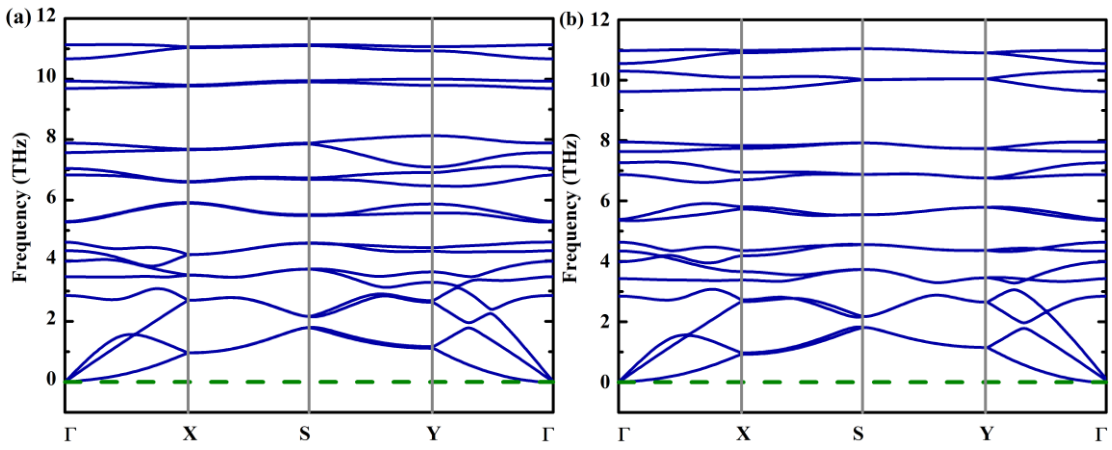

Figure S4 Calculated phonon dispersion curves of (a) *A* and (b) *B* monolayers.

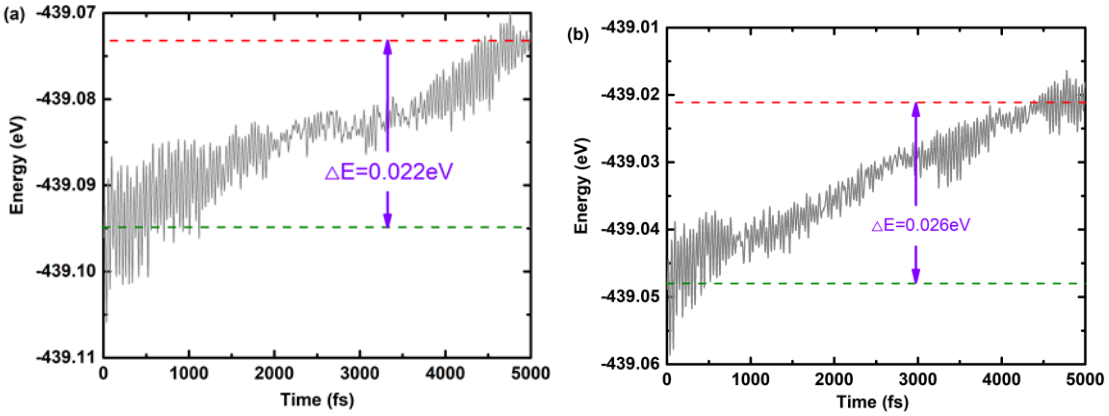

Figure S5 Total potential energy of monolayer (a) *A* and (b) *B* in AIMD.

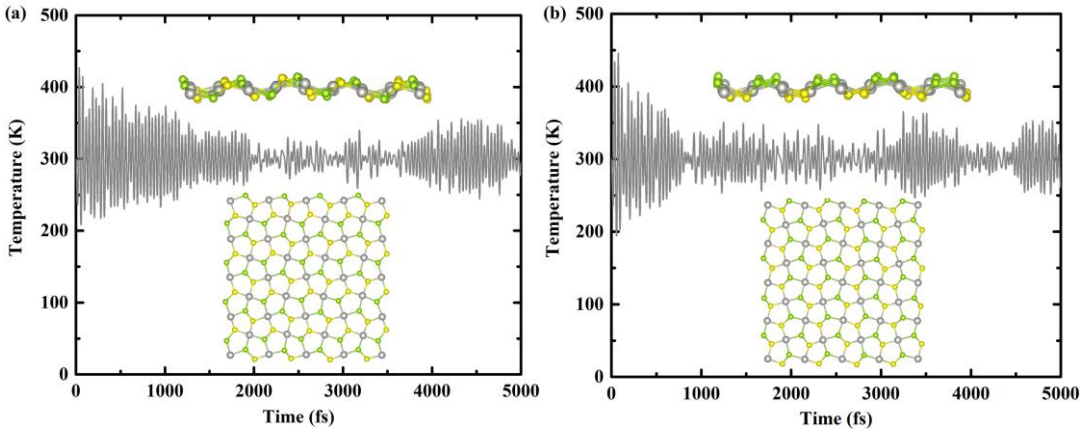

Figure S6 The temperature fluctuations with respect to AIMD steps at 300 K (using 4×4×1 supercell) and the snapshot of the PdSSe monolayer (a) *A* and (b) *B* at the end of 5 ps.

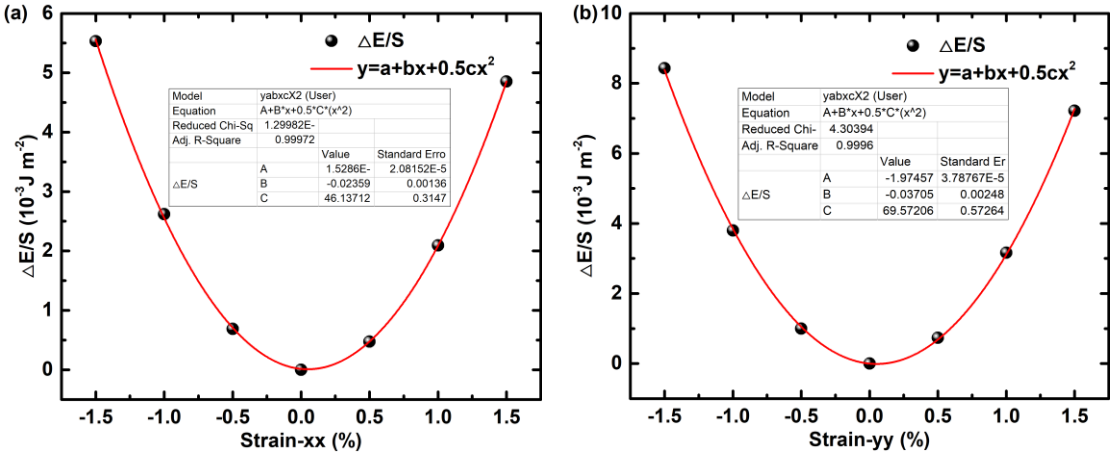

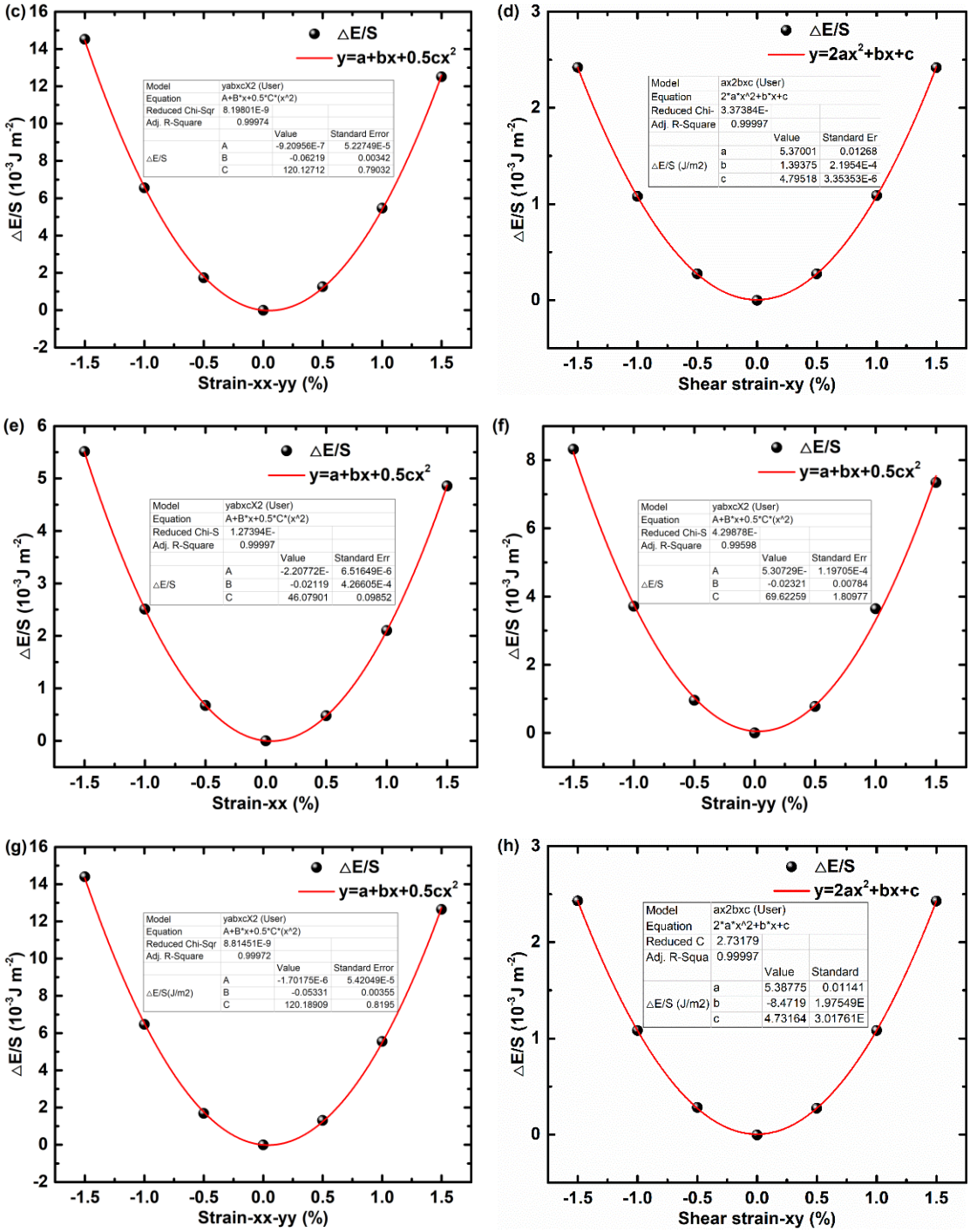

Figure S7 Introducing tiny deformation, the elastic constants are obtained by fitting the elastic energy per unit area and strain: in monolayer *A*, (a) *x* axial deformation for fitting C_{11}, (b) *y* axial deformation for fitting C_{22}, (c) hydrostatic planar deformation for fitting $C_{11} + C_{22} + 2C_{12}$ and (d) shear deformation for fitting C_{44}; the same manners of deformation in monolayer *B* to fit (e) C_{11}, (f) C_{22}, (g) $C_{11} + C_{22} + 2C_{12}$, and (h) C_{44}.

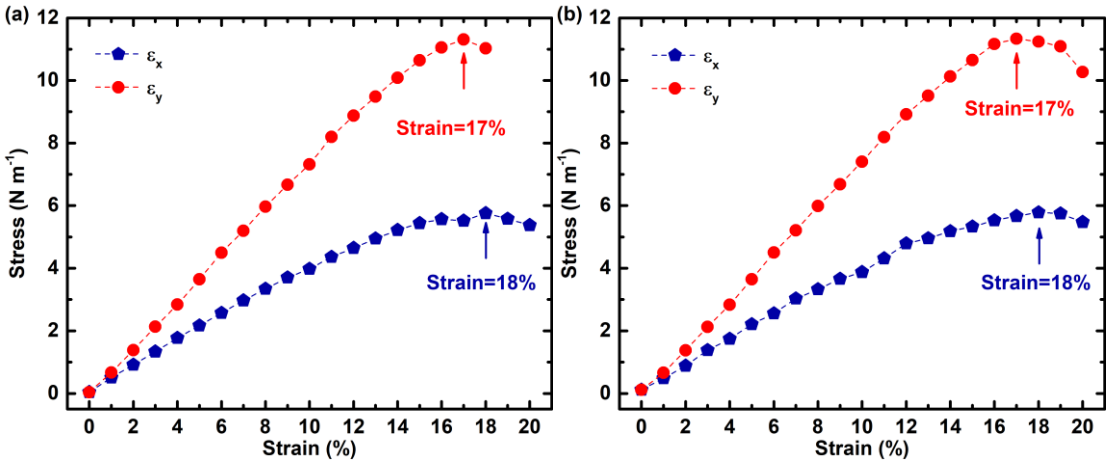

Figure S8 Calculated stress-strain relationship of monolayer *A* (a) and *B* (b) PdSSe. The arrows indicate the critical tensile strains (up to 18% and 17% for uniaxial strain in the *x* and *y* directions).

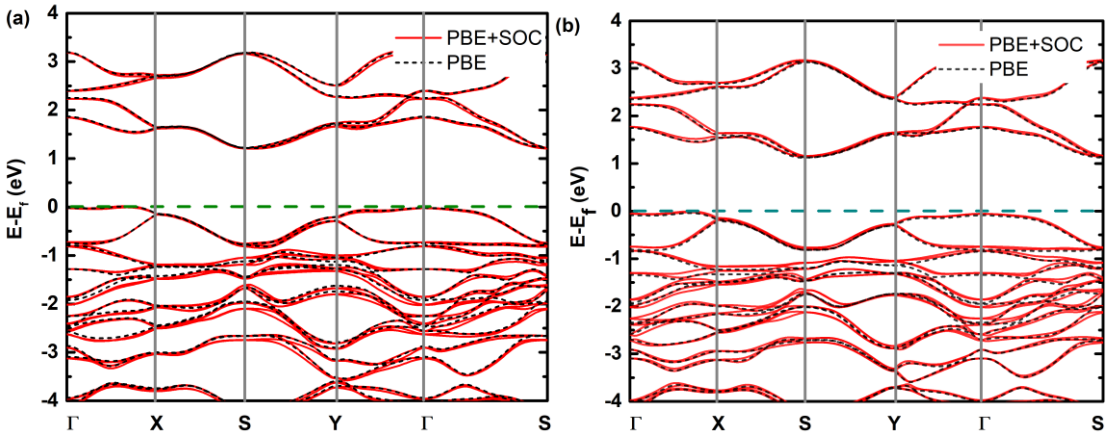

Figure S9 The band structures of monolayer (a) *A* and (b) *B* PdSSe calculated with PBE and PBE+SOC.

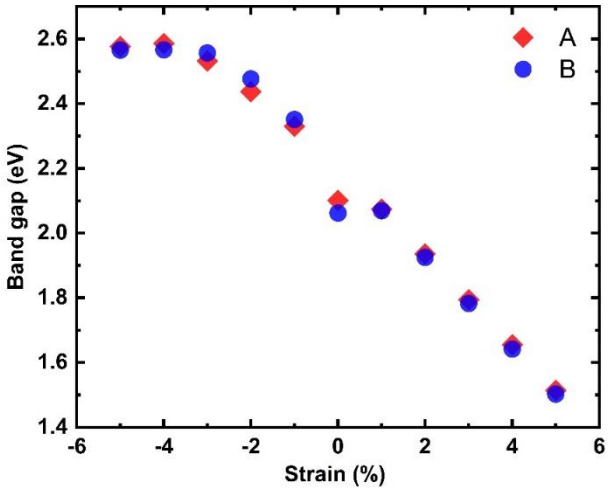

Figure S10 Band gap (calculated with HSE06) variations of the A and B monolayer PdSSe as a function of biaxial strain.

4. Comparisons of band gaps and optical properties with other candidate photocatalyst materials

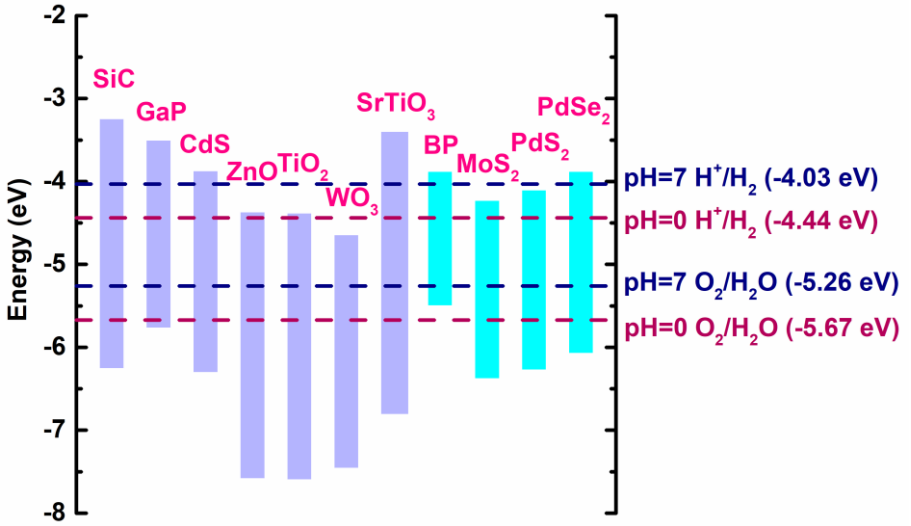

Figure S11 A comparison of band edge positions of common photocatalyst candidate semiconductors.[3] As a supplement, the band edge positions of the typical 2D materials BP and MoS_2, as well as the isostructural NMDCs materials PdX_2 are calculated and marked in blue (BP is short for black phosphorus).

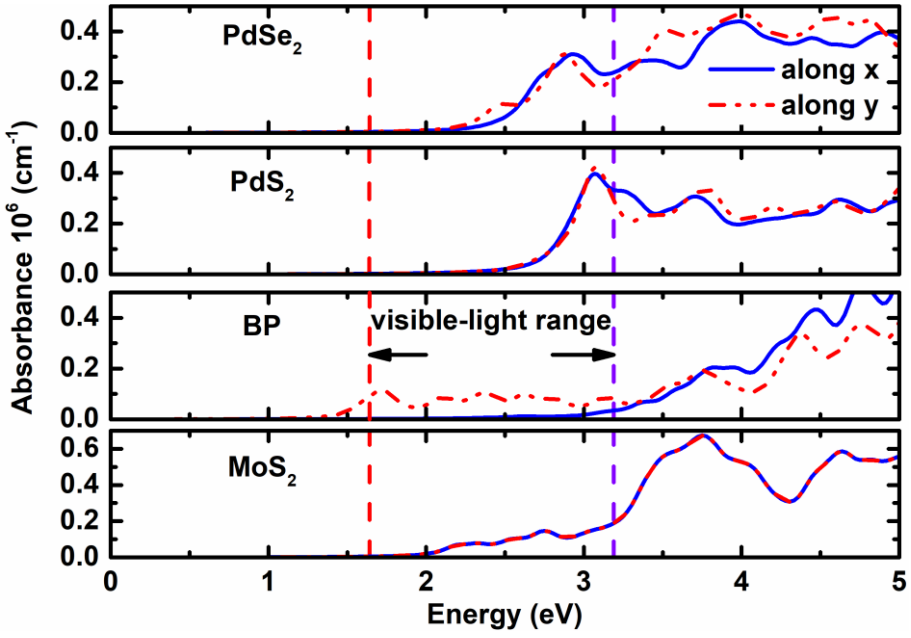

Figure S12 The light absorption coefficient of $PdSe_2$, PdS_2, BP (black phosphorus) and MoS_2.

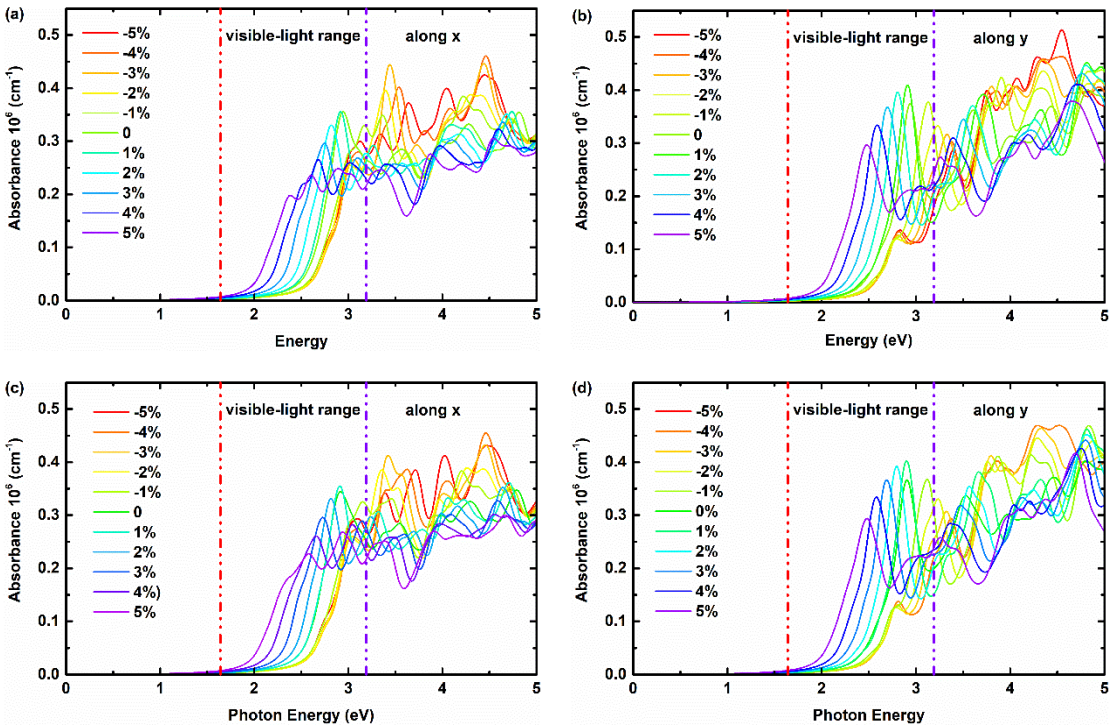

Figure S13 The light absorption coefficient of monolayer PdSSe under strains: *A* monolayer PdSSe along *x* (a) and *y* (b) directions; *B* monolayer PdSSe along *x* (c) and *y* (d) directions.

5. Fitting of in-plane elastic modulus C_{2d} and deformation potential constant E_1^i

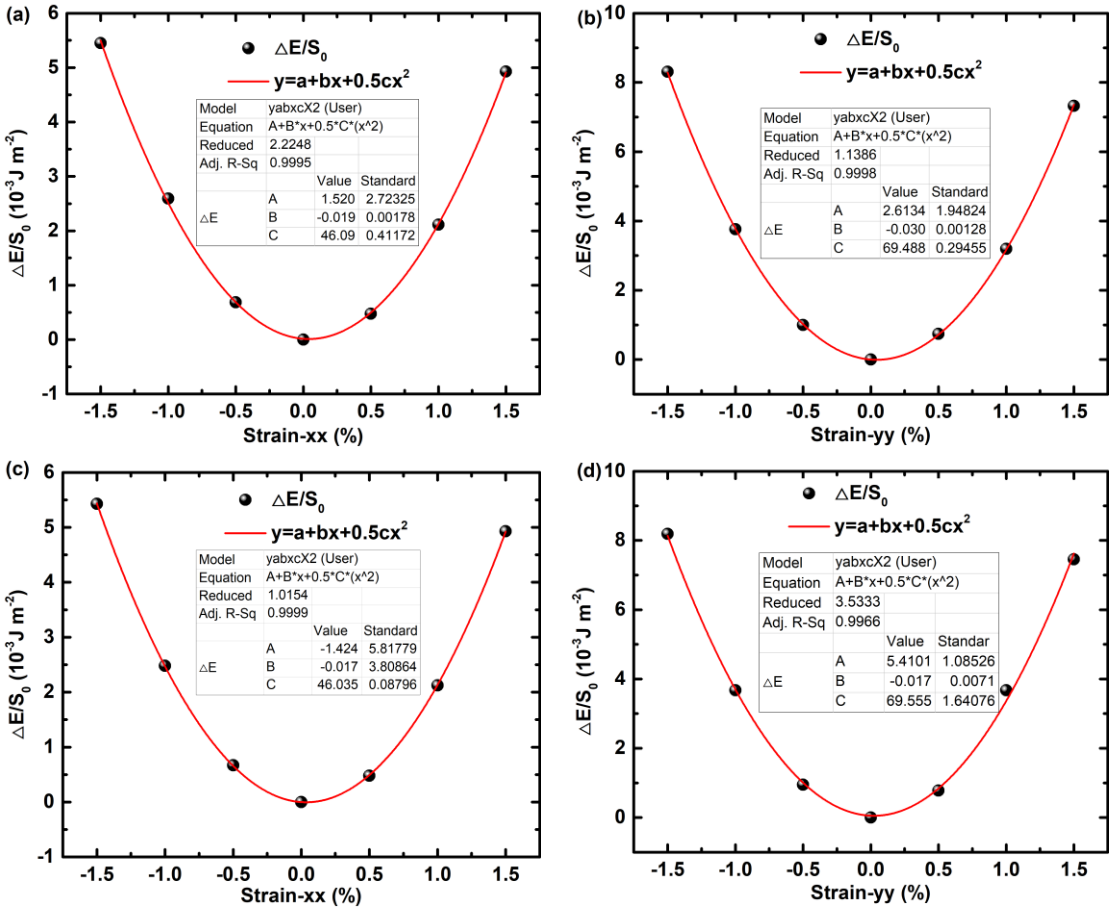

Figure S14 The in-plane elastic modulus C_{2d} is calculated by quadratic function fitting for monolayer *A* in the (a) *x* and (b) *y* directions; for monolayer *B* in the (c) *x* and (d) *y* directions.

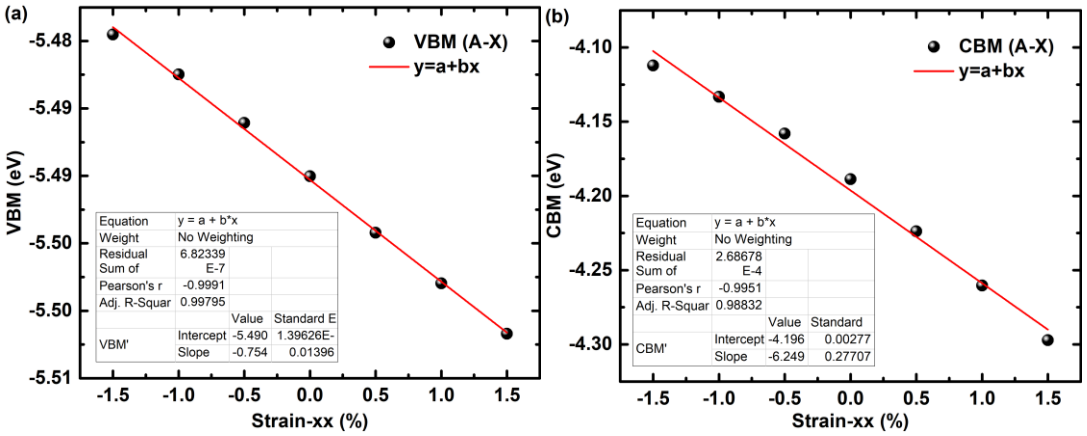

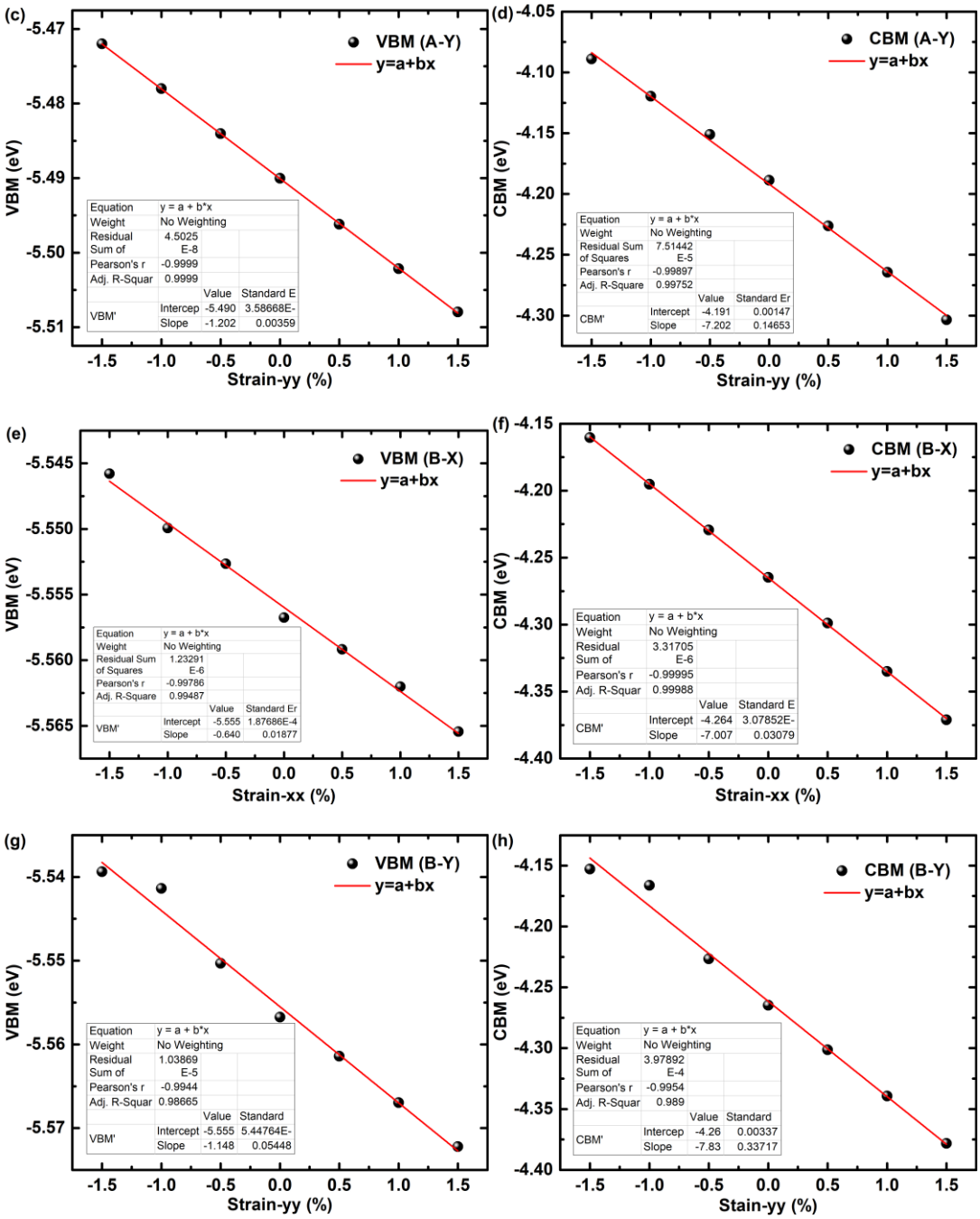

Figure S15 Fitting the deformation potential constant E_1^i for monolayer *A*: (a) *x* axis uniaxial strained VBM, (b) *x* axis uniaxial strained CBM, (c) *y* axis uniaxial strained VBM and (d) *y* axis uniaxial strained CBM; for monolayer *B*: (e) *x* axis uniaxial strained VBM, (f) *x* axis uniaxial strained CBM, (g) *y* axis uniaxial strained VBM and (h) *y* axis uniaxial strained CBM.

6. Water molecule adsorbed on the monolayer surface

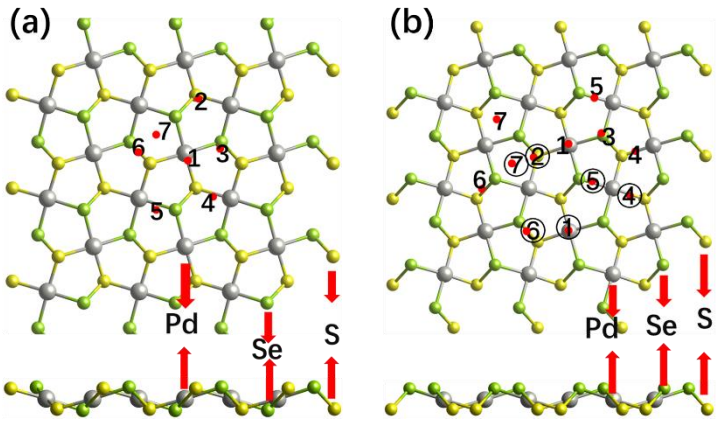

Figure S16 The initial adsorption positions of the H_2O molecules marked by the small red dot on the surface of monolayer *A* (a) and *B* (b). On the surface of Janus *B* monolayer, the adsorptions on the Se side are marked by a number with a small circle.

Table S4 Adsorption energy (eV) of water molecules on the surface of the PdSSe monolayers. B(S) and B(Se) represent the S and Se atomic side of the *B* monolayer, respectively. The most stable sites for two monolayers are highlight in red.

Surface/initial site	1	2	3	4	5	6	7
A	-0.053	-0.086	0.023	-0.076	0.041	0.052	-0.133
B(S)	0.143	0.035	-	-0.038	-0.102	-0.063	-0.151
B(Se)	-0.145	-	0.003	0.039	-0.162	0.010	-0.008

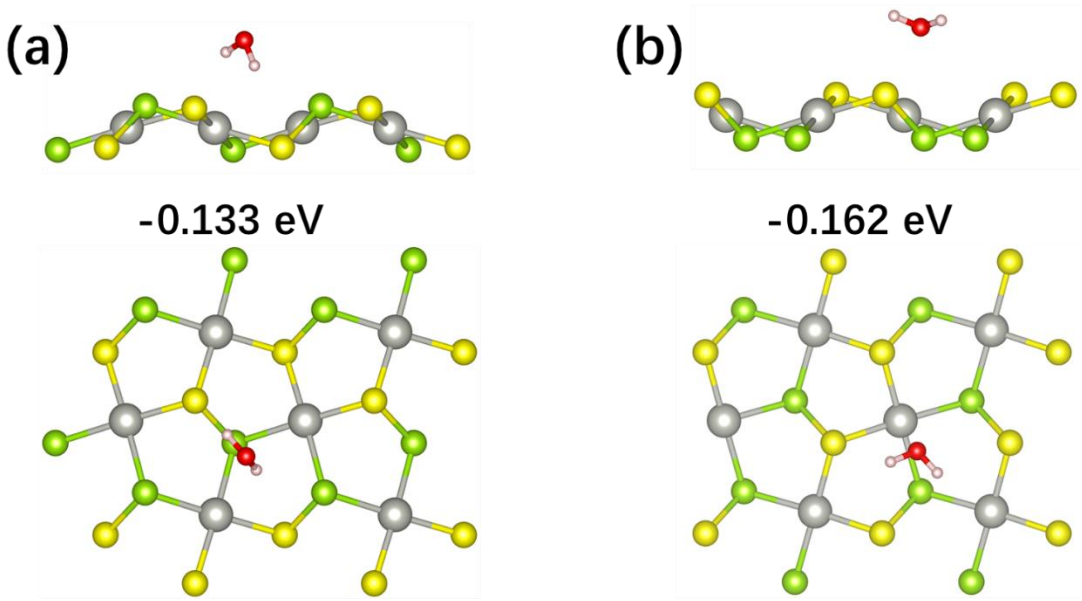

Figure S17 The most favorable adsorption configurations of the water molecules on the surface of monolayer *A* (a) and *B* (b). The energies in the figures are adsorption energies.

Reference

1 Grønvold, F., and E. Røst. The crystal structure of $PdSe_2$ and PdS_2. Acta Crystallographica, 1957, 10: 329-331

2 Hulliger, F. Electrical properties of some nickel-group chalcogenides. Journal of Physics and Chemistry of Solids, 1965, 26: 639-645

3 Tong, H., Ouyang, S., Bi, Y., Umezawa, N., Oshikiri, M., & Ye, J.. Nano-photocatalytic materials: possibilities and challenges. Advanced materials, 2012, 24: 229-251